DOI: 10.17344/acsi.2018.4224 *Acta Chim. Slov.* **2018,** *65,* 448–461

Scientific paper

Hydrothermal Synthesis of Novel Magnetic Plate-Like $Bi_2O_2CO_3/CoFe_2O_4$ Hybrid Nanostructures and Their Catalytic Performance for the Reduction of Some Aromatic Nitrocompounds

Parisa Zarringhadam and Saeed Farhadi*

Department of Chemistry, Lorestan University, Khoramabad 68151-44316, Iran

** Corresponding author: E-mail: sfarhadi1348@yahoo.com*
Tel: +986633120611, fax: +986633120618

Received: 27-01-2018

Abstract

Novel magnetically separable $Bi_2O_2CO_3/CoFe_2O_4$ nanocomposites were fabricated by a feasible hydrothermal route. Fourier transform infrared (FT-IR) spectroscopy, X-ray diffraction (XRD), scanning electron microscopy (SEM), energy dispersive X-ray spectroscopy (EDX), transmission electron microscopy (TEM), X-ray photoelectron spectroscopy (XPS), UV-vis diffuse reflectance spectroscopy (DRS), vibrating sample magnetometer (VSM), and N_2 adsorption–desorption analysis were employed to examine the structure, morphology, particle size, phase composition, optical and magnetic properties of the as-synthesized nanocomposites. The results of the findings showed demonstrated the successful coupling of spherical $CoFe_2O_4$ nanoparticles and plate–like $Bi_2O_2CO_3$ nanostructures. The catalytic performance of magnetic $Bi_2O_2CO_3/CoFe_2O_4$ nanocamposites was evaluated in the reduction of some aromatic nitrocompounds such as nitrophenols and nitroanilines by using sodium borohydride ($NaBH_4$) aqueous solution at room temperature. The $Bi_2O_2CO_3/CoFe_2O_4$ nanocamposite with 30 %wt. $CoFe_2O_4$ exhibited the best performance in the reduction of aromatic nitrocompounds with 100% conversion into the corresponding amino compounds within 15–30 min with rate constant of 0.10–0.24 min^{-1}. The effect of catalyst dosage was also investigated on the efficiency of reduction process. Furthermore, magnetic $Bi_2O_2CO_3/CoFe_2O_4$ nanocomposite could be easily removed by an external magnet from the reaction system.

Keywords: Plate-like $Bi_2O_2CO_3$; bismuth-based nanomaterials; cobalt ferrite, magnetic nanocomposite; catalytic reduction; nitrophenols

1. Introduction

Nitrophenols are one of the most organic pollutants in industrial and agricultural waste waters.[1,2] Nitrophenols and their derivatives are significant by-products produced from pesticides, herbicides and synthetic dyes.[3–5] Among them, 4-nitrophenol (4-NP) is well known to cause damage to the central nervous system, liver, kidney and both animal and human blood. Hence its removal from the environment is a crucial task.[6–10] On the other hand, the reduction of 4-NP to 4-aminophenol (4-AP) is essential in pharmaceutical industries for the manufacture of analgesic, antipyretic and other drugs, in photographic developer, corrosion inhibitor, anticorrosion lubricant, etc.[11,12] Over the past few decades, the catalytic reduction of nitrophonols using $NaBH_4$ as reducing agent in aqueous medium has received considerable attention as a relatively simple and clean method.[13] Many reports are available on the application of metal and metal oxides nanocatalysts for the reduction of nitrophenols in the presence of $NaBH_4$.[14–22] However, the separation of them from the reaction mixture is an important issue. In order to solve these problems, the magnetic separable nanocomposites such as Au/Fe_3O_4,[23] Ag@Pd satellites/Fe_3O_4,[24] Pt/Fe_3O_4/CNTs,[25] and $Fe_3O_4/SiO_2/Ag$[26] have been exploited for the catalytic reduction of nitrophenols in aqueous media. In such approaches, although nanocomposites showed improved recyclability but they suffered from one or more drawbacks such as the usage of expensive noble metals and the multi-step preparation procedures. Hence, the development of an alternative inexpensive, facile and easy-removal magnetic catalyst for the reduction of nitrophenols is highly desirable in the context of environmental and industrial concerns.

During the recent years, bismuth-based nanostructured materials, such as Bi_2O_3,[27] $BiVO_4$,[28] Bi_2WO_6,[29] Bi_2MoO_6,[30,31]

BiOX (X = Cl, Br, I), and so on,[32–34] have received a great deal of attention due to their unique catalytic and photocatalytic activities. Among these compounds, some studies have focused on the fabrication of bismuth subcarbonate ($Bi_2O_2CO_3$) and its composites.[35] Up to now, many kinds of $Bi_2O_2CO_3$-based hybrid composites such as $Bi_2O_2CO_3$/β-Bi_2O_3,[36] $Bi_2O_2CO_3$/MoS_2,[37] $Bi_2O_2CO_3$/BiOX (X= Cl, Br and I),[38–40] $Bi_2O_2CO_3$/Bi_2WO_6,[41] $Bi_2O_2CO_3$/Bi_2S_3,[42] $Bi_2O_2CO_3$/CdS,[43] $Bi_2O_2CO_3$/$BiPO_4$,[44] g-C_3N_4/$Bi_2O_2CO_3$,[45] Ag_2O/$Bi_2O_2CO_3$,[46] Ag/AgBr/$Bi_2O_2CO_3$,[47] Ag_3PO_4/$Bi_2O_2CO_3$,[48] Ag_2CO_3/$Bi_2O_2CO_3$[49] and MWCNTs/$Bi_2O_2CO_3$[50] have been successfully synthesized, which showed enhanced catalytic or photocatalytic stability and activity than $Bi_2O_2CO_3$ alone. But most of these composites are difficult to separate and recycle, seriously limiting their extensive application. Therefore, fabrication of well-defined and easy separated $Bi_2O_2CO_3$-based catalysts from the suspended reaction system via a simple process remains to be a great challenge. To overcome this shortfall, coupling $Bi_2O_2CO_3$ with magnetic materials is highly desirable. In this regard, spinel-type metal ferrites (MFe_2O_4) are known to have high magnetic performance as well as excellent chemical stability.[51] Among them, $CoFe_2O_4$ nanoparticles have a higher strong magnetic property, and therefore, $CoFe_2O_4$ based composites can be magnetically separable in a suspension by virtue of their own magnetic properties without any introduction of additional magnetic particles. Based on the previous studies, it can be expected that the modification of $Bi_2O_2CO_3$ with $CoFe_2O_4$ to form $Bi_2O_2CO_3$/$CoFe_2O_4$ nanocomposites may improve the catalytic activity and recyclability. Furthermore, their magnetic nature makes composites magnetically separable from the reaction mixture in a convenient manner. As far as we know, there is no report about $CoFe_2O_4$-modified $Bi_2O_2CO_3$ until now.

In this work, novel magnetically separable $Bi_2O_2CO_3$ / $CoFe_2O_4$ nanocomposits with high catalytic performance were synthesized via loading various amounts of $CoFe_2O_4$ nanoparticles on the surface of plate-like $Bi_2O_2CO_3$ nanostrucures by a hydrothermal method at 180 °C for 24 h. The structure, morphology, and optical properties of the obtained nanomaterials were characterized in detail. Then, the excellent catalytic activity of the as-prepared $Bi_2O_2CO_3$/ $CoFe_2O_4$ composite nanomaterials was evaluated by the reduction of 4-nitrophenol in the presence of aqueous $NaBH_4$ solution under ambient conditions. In addition, the possible reaction mechanism was proposed based on the experimental results. This study provides a promising candidate for efficient removal of nitrophenols from water by an environment-friendly and economical approach.

2. Experimental

2. 1. Materials

Bismuth nitrate pentahydrate ($Bi(NO_3)_3$ $5H_2O$, 98%), citric acid (98.5%), cobalt(II) nitrate hexahydrate ($Co(NO_3)_2$ $6H_2O$, 98%), iron(III) nitrat nanohydrate ($Fe(NO_3)_3$ $9H_2O$, 98%), sodium borohydride ($NaBH_4$, 98.5%), 2-nitrophenol (2-NP, 99%), 4-nitrophenol (4-NP, 98%), 2-nitroaniline (2-NA, 99%) and 4-nitroaniline (4-NA, 99%) were obtained from Merck chemical company and used as received without further purification. All other chemicals were of analytical grade, commercially available and used without further purification.

2. 2. Methods of Characterization

FT-IR spectra were recorded on a Schimadzu system FT-IR 8400S spectrophotometer in transmission mode from 4000 to 400 cm^{-1} using KBr pellets. the XRD patterns of the samples were obtained on an X-ray diffractometer (Rigaku D-max C III) using Ni-filtered Cu Kα radiation (λ = 1.5406 Å) UV–vis diffuse reflection spectroscopy (DRS) was performed on a Snico S4100 spectrophotometer over the spectral range 200–1000 nm by using $BaSO_4$ as the reference. The shapes and morphologies of samples were observed by a MIRA3 TESCAN field emission scanning electron microscope (FESEM) equipped with a link energy-dispersive X-ray (EDX) analyzer. The particle size was determined by a CM120 transmission electron microscope (TEM) at an accelerating voltage of 80 kV. TEM samples were prepared by dropping the ethanol dispersion on a carbon coated copper grid. A PHS-1020 PHSCHINA instrument was used to measure the Brunauer-Emmett-Teller (BET) surface areas of the samples at liquid nitrogen temperature (77 K). Specific surface area calculations were made using Brunauer-Emmett-Teller (BET) method at the relative pressure (p/p_0) between 0.05 and 0.35. Magnetic measurements were carried out at room temperature using a vibrating sample magnetometer (VSM, Magnetic Daneshpajoh Kashan Co., Iran) with a maximum magnetic field of 10 kOe. X-ray photoelectron spectroscopy (XPS) was conducted using a thermo Scientifi, ESCALAB 250Xi, Mg X-ray resource instrument. UV-vis spectra of nitro compounds during the reduction reaction in aqueous solutions were analyzed using a Cary 100 double beam spectrophotometer operated at a resolution of 2 nm with quartz cells with path length of 1 cm in the wavelength range of 200 to 600 nm.

2. 3. Preparation of $CoFe_2O_4$ Nanoparticles

$CoFe_2O_4$ nanoparticles were prepared by hydrothermal process. $Fe(NO_3)_3$ $9H_2O$ (1.72 g) and $Co(NO_3)_2$ $6H_2O$ (0.62 g) were dissolved in 25 mL distilled water (Co/Fe mole ratio of 1:2), and then the solution was adjusted to a pH of 12 with NaOH (6 M). After stirring for 60 min, the mixture was transferred to a 50 mL Teflon-lined stainless steel autoclave and maintained at 180 °C for 12 h before being cooled down in air. The resulting precipitate was filtered, washed with deionized water and ethanol, and dried at 60 °C for 6 h.

2. 4. Preparation of Plate-Like $Bi_2O_2CO_3$ Nanoparticles

To obtain plate-Like $Bi_2O_2CO_3$ nanoparticles, 2.0 mmol of bismuth nitrate pentahydrate [Bi $(NO_3)_3$ $5H_2O$] was dissolved in 20 mL of HNO_3 aqueous solution (1 M), and then 1.5 mmol of citric acid ($C_6H_8O_7$) was added under magnetic stirring. The pH of the solution was adjusted to 6 by adding NaOH aqueous solution (2 M) under magnetic stirring. Finally, the white-colored precursor suspension was transferred into a 50 mL Teflon-lined stainless steel autoclave and heated for 24 h at 180 °C. After hydrothermal treatment, the autoclave was cooled down to room temperature naturally. The resulting precipitate was collected by centrifugation, washed with deionized water several times, and dried at 60 °C for 6 h.

2. 5. Preparation of $Bi_2O_2CO_3/CoFe_2O_4$ Nanocomposites

To synthesize $Bi_2O_2CO_3/CoFe_2O_4$ nanocomposites, 2.0 mmol of $Bi(NO_3)_3$ $5H_2O$ was dissolved in 20 mL of HNO_3 (1 M), and then 1.5 mmol of citric acid ($C_6H_8O_7$) was added under magnetic stirring. The pH of the solution was adjusted to 6 by adding NaOH aqueous solution (2 M) under magnetic stirring. Then, the required amount of $CoFe_2O_4$ nanoparticles (30 and 45 wt%) was added to the $Bi_2O_2CO_3$ precursor suspension. After sonication for 30 min, the homogenized suspension was transferred into a 50 ml Teflon-lined stainless steel autoclave, sealed and maintained at 180 °C for 24 h. Then, the autoclave was naturally cooled down to room temperature and the resulting precipitate was separated by a magnet, washed with deionized water several times, dried at 60 °C and used for further characterization. The obtained samples with 30 and 45 wt% $CoFe_2O_4$ nanoparticles were denoted as $Bi_2O_2CO_3/CoFe_2O_4$30% and $Bi_2O_2CO_3/CoFe_2O_4$45%, respectively.

2. 6. Catalytic Tests

The catalytic performance of the synthesized $Bi_2O_2CO_3/CoFe_2O_4$ nanocomposites in the reduction of 4-nitrophenol (4-NP) to 4-amiophenol (4-AP) was evaluated by excess aqueous $NaBH_4$ solution at room temperature. In a typical catalytic reaction, 2 mL of aqueous solution of 4-NP (0.2 mM) and 0.5 mL of freshly prepared aqueous solution of $NaBH_4$ (20 mM) were mixed together in a standard quartz cell, having 1 cm path length. The solution color turned to bright yellow rapidly. Then, 5 mg of the $Bi_2O_2CO_3/CoFe_2O_4$ nanocomposite was added and stirred at room temperature. The solution was quickly subjected to UV–Vis measurements; Afterward, the absorbance of the solution was in situ measured every several minutes (2 min) in the scanning range of 200–500 nm to obtain the successive change about the reaction. In order to optimized the catalyst amount, similar experiments have been carried out in the presence of various amount of the catalyst (2.5, 5, 10, 15, and 20 mg in 2.5 mL aqueous solutions) on the reduction of 4-NP. The reduction of 2-nitrophenol (2-NP) and 2-nitroaniline (2-NA) and 4-nitroaniline (4-NA) was also carried out under the same conditions. For comparison, similar experiment was performed in the presence of the pure $Bi_2O_2CO_3$ (5 mg) and $CoFe_2O_4$ (5 mg) catalysts. For recycling experiments, the $Bi_2O_2CO_3/CoFe_2O_4$ catalyst was recovered from the solution by an external magnet after completion of the reaction. The magnetically recovered catalyst was washed repeatedly with deionized water, dried at 60 °C and then employed for a new run.

3. Results and Discussion

3. 1. Characterization of $Bi_2O_2CO_3/CoFe_2O_4$ Nanocomposites

FT-IR spectra of the as-prepared $Bi_2O_2CO_3$, $CoFe_2O_4$ and $Bi_2O_2CO_3/CoFe_2O_4$ samples are indicated in Figure 1. For pure $Bi_2O_2CO_3$ sample in Figure 1(a), the sharp peaks at *ca.* 1400 and 845 cm^{-1} are the characteristic stretching

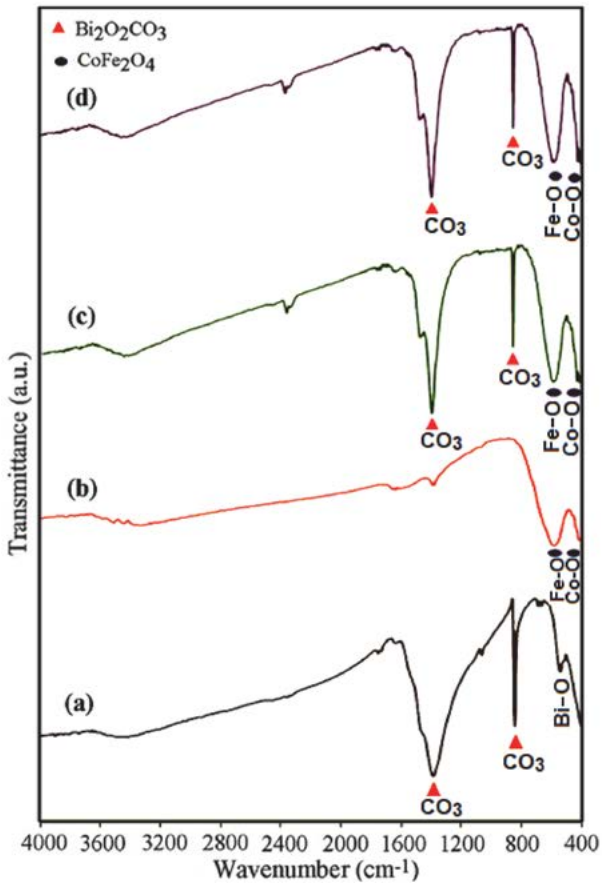

Figure 1. FT-IR spectra of (a) $Bi_2O_2CO_3$, (b) $CoFe_2O_4$ (c) $Bi_2O_2CO_3/CoFe_2O_4$30%, and (d $Bi_2O_2CO_3/CoFe_2O_4$45%.

and bending vibrations of CO_3^{2-} groups, respectively.[52] Meanwhile, the intensive peak at about 550 cm^{-1} was attributed to the stretching vibration of the Bi-O, suggesting the formation of $Bi_2O_2CO_3$.[53] In the case of $CoFe_2O_4$ (Figure 1(b)), the two peaks appeared at 603 and 458 cm^{-1} are related to the stretching vibrations of M–O bonds in the tetrahedral and octahedral sites of spinel-type oxide, respectively.[54,55] FT-IR spectra of the $Bi_2O_2CO_3/CoFe_2O_4$ nanocomposites in Figures 1(c) and (d) show the stretching and bending vibrations correspond to the carbonate group (CO_3^{2-}) in $Bi_2O_2CO_3$ at 1400 and 844 cm^{-1}, besides strong bands of $CoFe_2O_4$ in the 400–600 cm^{-1} range. This finding demonstrates the coexistence of $Bi_2O_2CO_3$ and $CoFe_2O_4$ in the nanocomposites.

The crystal structure of samples was further characterized using XRD. Figure 2 shows the XRD patterns of the $Bi_2O_2CO_3$, $CoFe_2O_4$ and $Bi_2O_2CO_3/CoFe_2O_4$ nanocomposites with different contents of $CoFe_2O_4$. The patterns of Figures 2(a) and (b) are well consistent with the tetragonal $Bi_2O_2CO_3$ phase (JCPDS no. 41–1488) and the spinel-type $CoFe_2O_4$ phase (JCPDS no. 01–1121). As shown in Figures 2(c) and (d), all the $Bi_2O_2CO_3/CoFe_2O_4$ samples exhibit a coexistence of both $Bi_2O_2CO_3$ and $CoFe_2O_4$ phases without any impurity phase, indicating successful synthesis of composites. In addition, the intensity of characteristic $CoFe_2O_4$ peaks at 2θ = 35.76 and 63.13 in nanocomposite increased with increasing $CoFe_2O_4$ amount. Besides, the diffraction peaks of $Bi_2O_2CO_3/CoFe_2O_4$ nanocomposites exhibited sharp and intense state, indicating a promising crystalline nature which was beneficial for the following catalytic activity.

The shape and morphology of the as-synthesized $CoFe_2O_4$, $Bi_2O_2CO_3$ and $Bi_2O_2CO_3/CoFe_2O_4$ samples were investigated by FE-SEM. The SEM images of $CoFe_2O_4$ sample in Figures 3(a) and (b) show a large quantity of nearly uniform monodispersed spheres with an average diameter of about 15 nm. The SEM images in Figures 3(c) and (d) show that the bare $Bi_2O_2CO_3$ sample was formed from plate-like particles which were loosely aggregated. As can be observed, the porous structure was formed by self-assembly of these nanoplates. SEM images of the $Bi_2O_2CO_3/CoFe_2O_4$ nanocomposites containing 30% and 45% of $CoFe_2O_4$ are shown in Figures 3(e) and (f), respectively. It is evident that the shape and morphology of $Bi_2O_2CO_3/CoFe_2O_4$ nanocomposits are similar to those of the pure $Bi_2O_2CO_3$, but many spherical $CoFe_2O_4$ nanoparticles are seen on the surface of plate-like $Bi_2O_2CO_3$ nanostructures. From images, it can be clearly seen that a lot of

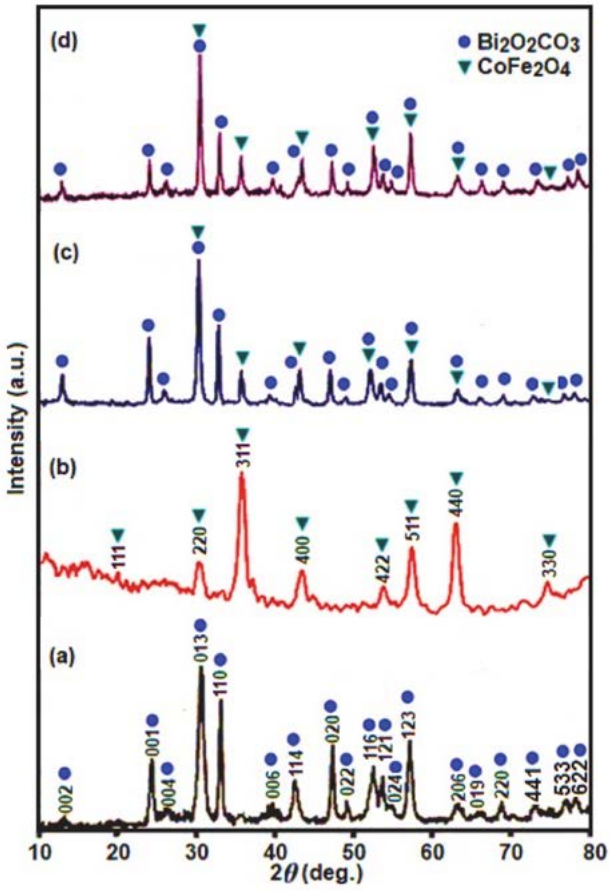

Figure 2. XRD patterns of (a) $Bi_2O_2CO_3$, (b) $CoFe_2O_4$, (c) $Bi_2O_2CO_3/CoFe_2O_4$30%, and (d) $Bi_2O_2CO_3/CoFe_2O_4$45%.

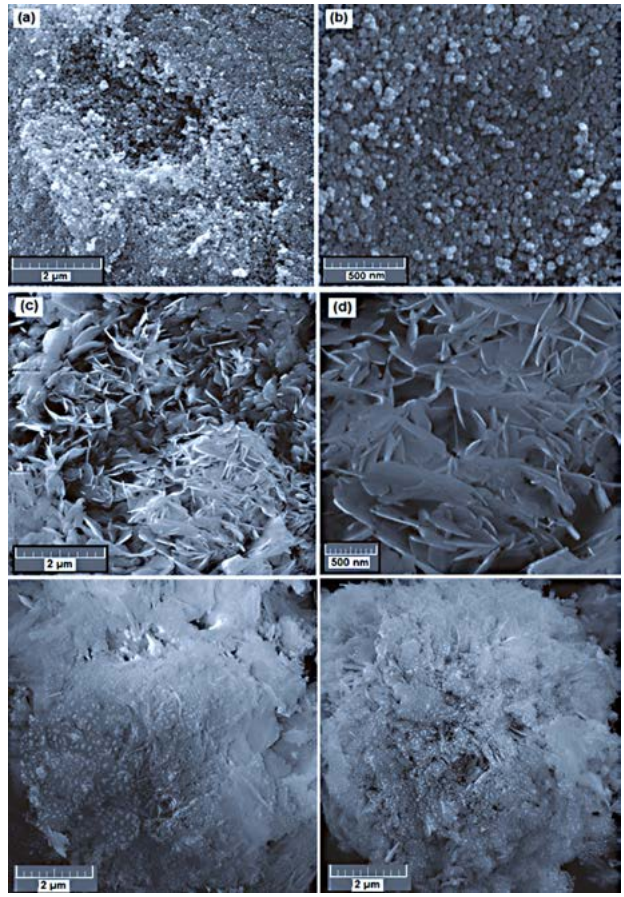

Figure 3. SEM images of (a and b) $CoFe_2O_4$, (c and d) $Bi_2O_2CO_3$, (e) $Bi_2O_2CO_3/CoFe_2O_4$30% (f) $Bi_2O_2CO_3/CoFe_2O_4$45% samples.

spherical $CoFe_2O_4$ nanoparticles with a size of about 15–20 nm were well deposited on the $Bi_2O_2CO_3$ nanoplates.

The size and microstructure of the as-prepared $Bi_2O_2CO_3/CoFe_2O_4$ samples were further investigated by TEM. The sample powder was sonicated in ethanol for 30 min and a drop of the suspension was dried on a carbon-coated microgrid for TEM measurements. The TEM images in Figure 4(a)-(c) show that the obtained $Bi_2O_2CO_3/CoFe_2O_4$30% nanocomposite was formed mainly from plate-like particles with a weak agglomeration. Also, from the TEM images in Figure 4(d), it is clear that the $Bi_2O_2CO_3/CoFe_2O_4$45% consists of plate-like structure with the lengths of 15–40 nm and thicknesses of several nanometers while $CoFe_2O_4$ nanoparticles show sphere-like shapes. It is obvious from the TEM images that the nanoplates exhibit mostly square-like shapes, although some are rectangular. As can be observed on all images, many spherical $CoFe_2O_4$ dark-color particles are observed to be deposited on the surface of bright plates of the $Bi_2O_2CO_3$. The average size of $CoFe_2O_4$ particles was calculated to be 15 nm from the measurements on the TEM micrographs which is in close agreement with the size obtained from XRD analysis. It is clear from the images, the morphology of the $Bi_2O_2CO_3/CoFe_2O_4$ composites from TEM images agreed with the SEM results.

The energy dispersive X-ray spectroscopy (EDX) was used to characterize the elemental composition of the as-prepared samples. The EDX spectra of $CoFe_2O_4$, $Bi_2O_2CO_3$ and $Bi_2O_2CO_3/CoFe_2O_4$30% are shown in Figure 5. The EDX spectrum of $CoFe_2O_4$ in Figure 5(a) shows the existence of Co, Fe and O elements as well as the EDX spectrum of $Bi_2O_2CO_3$ (Figure 5(b)) shows the existence of Bi, C and O elements. In addition, the constituents of $Bi_2O_2CO_3/CoFe_2O_4$30% were studied by EDX method. As shown in Figure 5(c), the EDX elemental spectrum of the nanocomposite sample exhibits elemental peaks corresponding to both $CoFe_2O_4$ and $Bi_2O_2CO_3$ and no other impure peaks can be observed, indicating that the composite sample is consisted of $CoFe_2O_4$ and $Bi_2O_2CO_3$. In all samples, the presence of Au peak at 2.2 KeV is due to SEM-EDX sample holder.

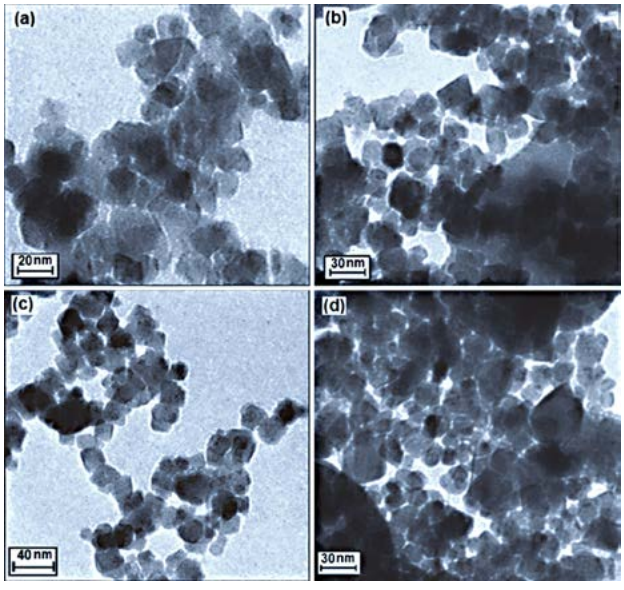

Figure 4. TEM images of (a)-(c) $Bi_2O_2CO_3/CoFe_2O_4$30%, and (d) $Bi_2O_2CO_3/CoFe_2O_4$45% samples.

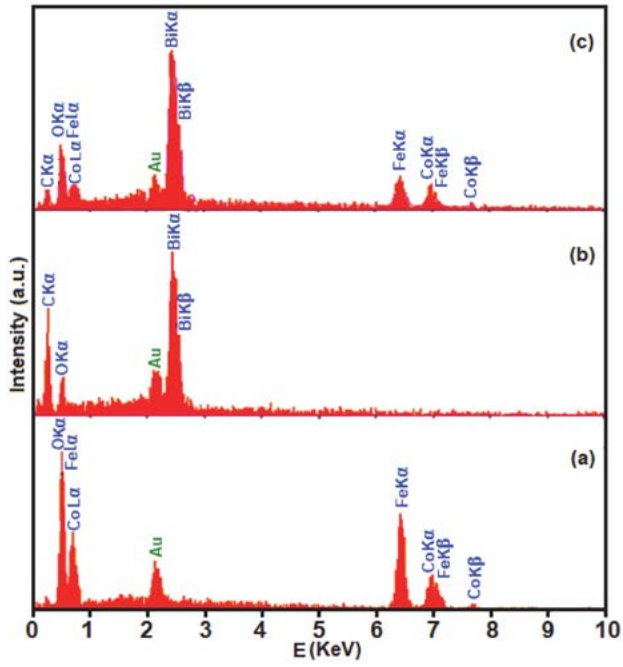

Figure 5. EDX spectra of (a) $CoFe_2O_4$, (b) $Bi_2O_2CO_3$ and (c) $Bi_2O_2CO_3/CoFe_2O_4$30% nanocomposite.

To further determine the composition and element distributions of $Bi_2O_2CO_3/CoFe_2O_4$30% composite, EDX mapping measurements were also carried out. Figure 6 shows a representative SEM image of the nanocomposite with corresponding EDX elemental mappings. From the maps in Figure 6(b)-(f), can be observed that the Bi, C, O, Co and Fe elements are uniformly distributed over the sample, confirming the homogeneity of the nanocomposite. The EDX elemental mappings of the $Bi_2O_2CO_3/CoFe_2O_4$30% composite (Figures 6(e) and (f)) display that the elements of Co and Fe from $CoFe_2O_4$ phase are distributed on the surface of the $Bi_2O_2CO_3$. The EDX mappings results further indicate that the $Bi_2O_2CO_3/CoFe_2O_4$ nanocomposites have been successfully synthesized.

The optical properties of the as-prepared $Bi_2O_2CO_3$, $CoFe_2O_4$ and $Bi_2O_2CO_3/CoFe_2O_4$ composites were investigated by the diffuse reflectance UV-vis spectra (DRS) absorption spectroscopy (Figure 7). Figure 7(a) displays the UV-vis diffuse reflectance spectra of the bare $Bi_2O_2CO_3$ (curve i), $Bi_2O_2CO_3/CoFe_2O_4$30% composite (curve ii) and $CoFe_2O_4$ (curve iii). Bare $Bi_2O_2CO_3$ shows absorption edge at ~400 nm whereas pure $CoFe_2O_4$ shows good absorbance in the visible light region up to 490 nm. As can be

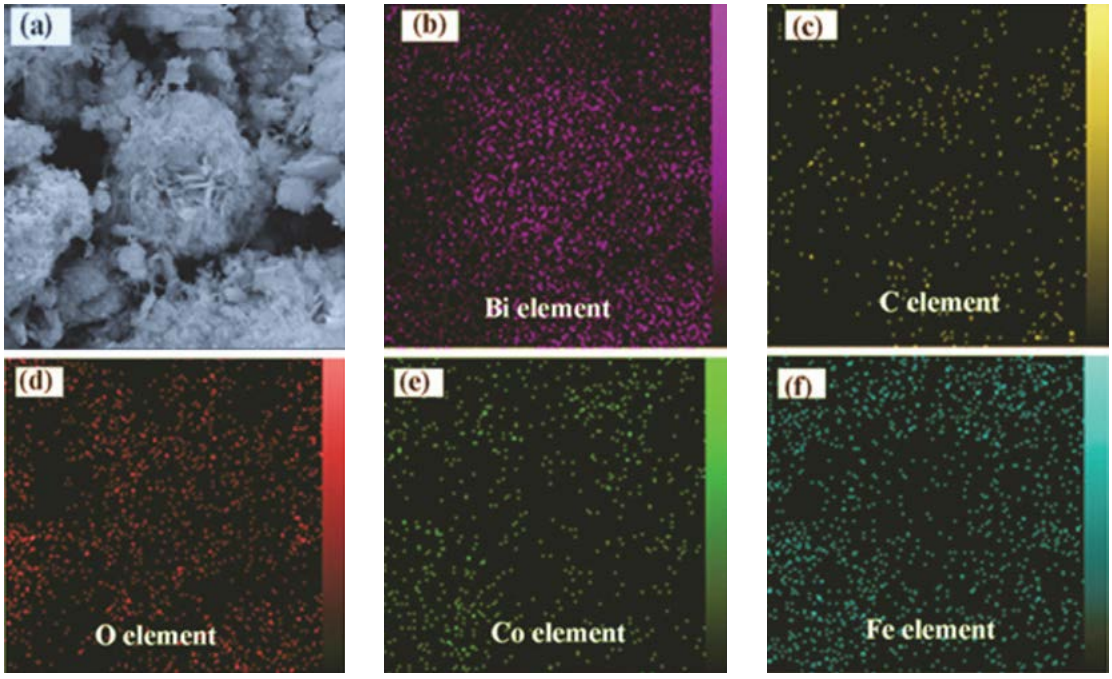

Figure 6. SEM image and the corresponding elemental mapping images of $Bi_2O_2CO_3/CoFe_2O_4$30%.

seen in curve ii of Figure 7(a), the UV-vis band of $Bi_2O_2CO_3/CoFe_2O_4$ nanocomposite indicates an enhancement in absorption intensity in the visible region together with a red shift, compared to that of the pure $Bi_2O_2CO_3$ due to the coupling with $CoFe_2O_4$ phase. The band gaps (Egs) of these three samples were calculated by the following formula based on the DRS results:[57]

$$(\alpha h\nu)^{1/2} = B(hv\text{-}Eg) \quad (1)$$

Where α, h, ν and B are absorption coefficient, plank constant, light frequency, and a constant, respectively. Therefore, Eg value of the samples can be estimated from a plot $(\alpha h\nu)^{1/2}$ versus photon energy (hv). The intercept of the tangent to the x axis would give an approximation of the band-gap energy of the samples (Figure 7(b)). As shown in Figure 7(b) (curves i-iii), the Eg values of pure $Bi_2O_2CO_3$, $Bi_2O_2CO_3/CoFe_2O_4$30% nanocomposite and pure $CoFe_2O_4$ were found to be 3.49, 2.89 and 2.79 eV, respectively. It is clear that the $Bi_2O_2CO_3/CoFe_2O_4$30% composite shows a band gaps at 2.89 eV with a red shift compared to that of the pure $Bi_2O_2CO_3$ (3.49 eV), indicating formation of hybrid heterostructures.

The elemental composition and oxidation states of $Bi_2O_2CO_3/CoFe_2O_4$30% sample were carefully analyzed by XPS. The full XPS spectrum in Figure 8(a) shows that the

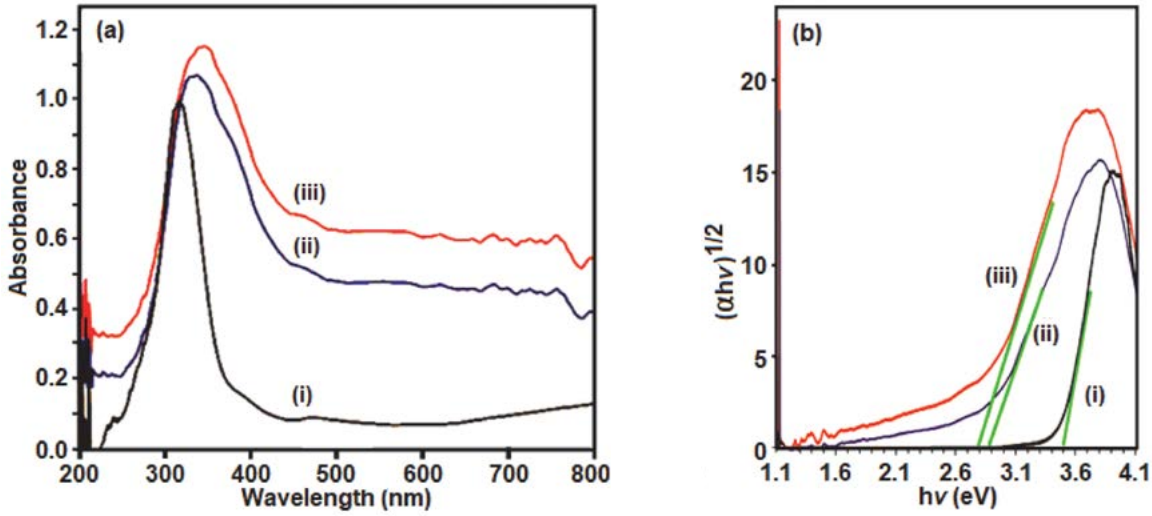

Figure 7. (a) UV-vis diffuse reflectance spectra and (b) $(\alpha h\nu)^2$ versus hν curves of (i) pure $Bi_2O_2CO_3$ (ii) $Bi_2O_2CO_3/CoFe_2O_4$30% and (iii) $CoFe_2O_4$.

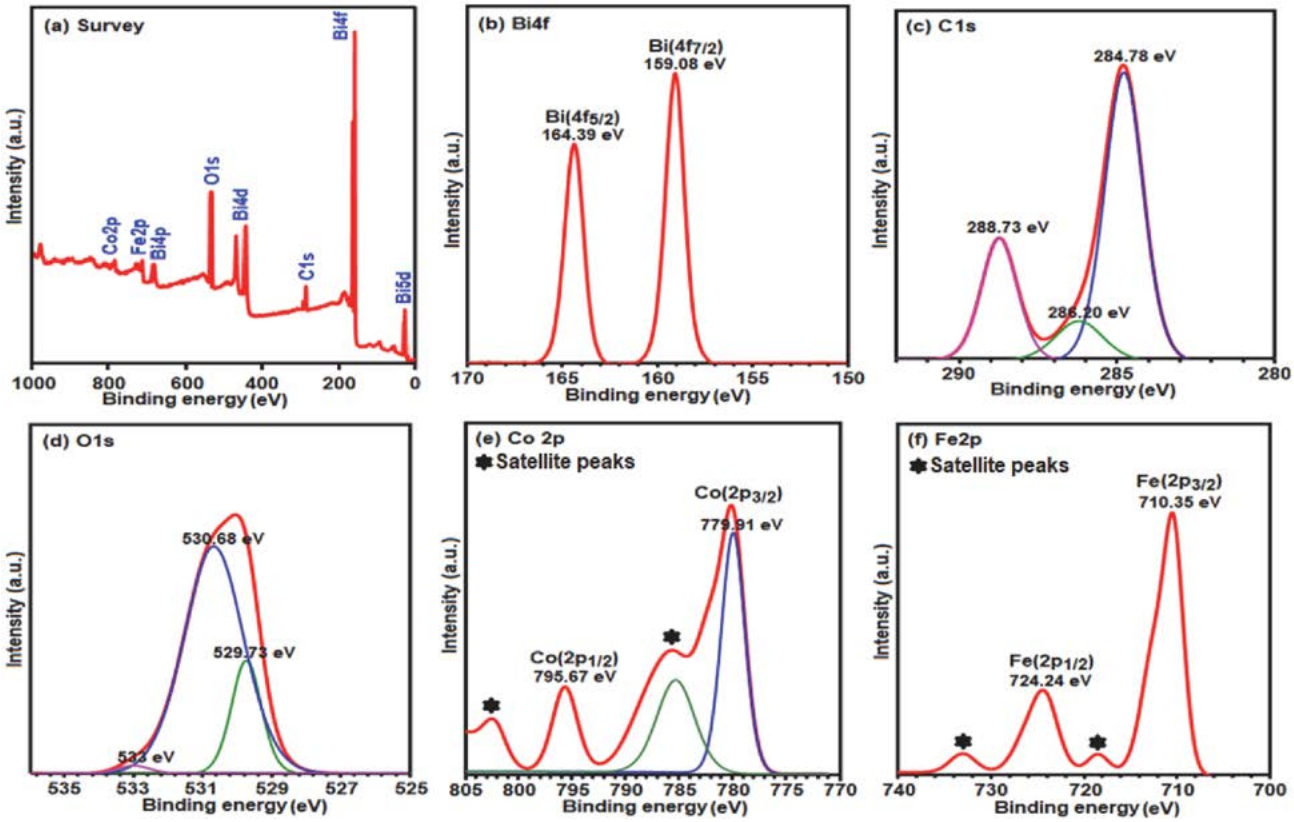

Figure 8. (a) XPS survey spectrum of the $Bi_2O_2CO_3/CoFe_2O_4$30% nanocomposite. High-resolution XPS spectra of (b) Bi 4f, (c) C 1s, (d) O 1s, (e) Co 2p and (f) Fe 2p.

sample consists of Bi, O, C, Co and Fe elements, in consistent with the EDX results. In order to further investigate the chemical state of each element, the high-resolution XPS spectra of Bi 4f, C 1s, O 1s, Co 2p and Fe 2p for the as-prepared $Bi_2O_2CO_3/CoFe_2O_4$30% are separately shown in Figure 8(b)-(e). As shown in Figure 8(b), the peaks located at binding energies of 159.08 and 164.39 eV are attributed to Bi $4f_{7/2}$ and Bi $4f_{5/2}$, respectively, indicating the existence of Bi^{3+} ions in the sample.[58] In Figure 8(c), the peak at 284.78 eV is attributed to carbon reference, while the peak at 288.73 eV corresponds to the carbon of carbonate ion (CO_3^{2-}) in $Bi_2O_2CO_3$.[58] For the oxygen element (Figure 8(d)), the O 1s peaks are well fitted into three different peaks at 529.73 eV, 530.68eV and 532 eV. According to the experiment results, the peak located at 529.73 eV is arisen from Bi-O in $Bi_2O_2CO_3$ while that at 530.63 eV is from CO_3^{2-} species and $CoFe_2O_4$.[59] Other small peak at higher binding energy of 532 eV can be attributed to the presence of surface-chemisorbed adsorbed H_2O.[60] As shown in Figure 8(e), the peaks at 979.91 eV and 795.67 eV could be assigned to Co $2p_{3/2}$ and Co $2p_{1/2}$, respectively, shouldering with satellite peaks at 785.29 eV and 802.27 eV. Figure 8(f) shows Fe 2p peaks at binding energies of 710.35 eV (Fe $2p_{3/2}$) and 724.24 eV (Fe $2p_{1/2}$) with weak satellite peaks at 718.50 eV and 733.04 eV. The observed Co 2p and Fe 2p photoelectron peaks are consistent with those reported for Co^{2+} and Fe^{3+} in $CoFe_2O_4$.[61] The above results can powerfully support the presence of $CoFe_2O_4$ in the as-prepared $Bi_2O_2CO_3/CoFe_2O_4$ sample, implying the formation of heterojunction between $CoFe_2O_4$ and $Bi_2O_2CO_3$ in the resulted composite.

The BET surface area and porous structure of the $Bi_2O_2CO_3/CoFe_2O_4$ composite were investigated based on nitrogen adsorption–desorption. Figure 9 gives the adsorption–desorption isotherms and the corresponding pore size distribution curve of the $Bi_2O_2CO_3/CoFe_2O_4$30% sample. As observed in Figure 9, the sample shows a type-III isotherm according to the IUPAC classification.[62] The isotherm shows a distinct H3 hysteresis loop in the relatively high pressure range (p/p_0 = 0.8–1). Generally, it is believed that the H3 hysteresis loop is related to the mesopores through the aggregates of plate-like particles which were further observed from the corresponding pore size distribution curve in the inset of Figure 9.[63] The obtained BET specific surface area of the $Bi_2O_2CO_3/CoFe_2O_4$30% sample is 88.09 $m^2\ g^{-1}$, whereas that of the $Bi_2O_2CO_3$ sample is 8.7 $m^2\ g^{-1}$.[63] Accordingly, it is clear that the BET surface area of the $Bi_2O_2CO_3/CoFe_2O_4$30% catalyst is much larger (about 10 times) than that of pure $Bi_2O_2CO_3$. The increased surface area may be also beneficial for the increase of active sites and catalytic activities. The total pore volume is 0.297 cm^3/g and the average pore size of this sample is 1.27 nm, which is estimated using the Barrett–Joyner–Halenda (BJH) method from the ad-

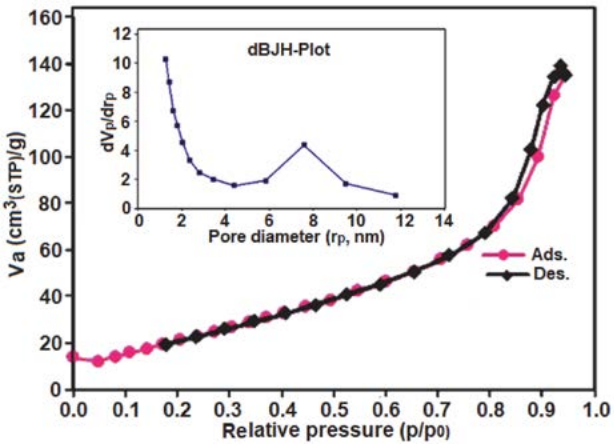

Figure 9. N_2 adsorption–desorption isotherm of the $Bi_2O_2CO_3$/$CoFe_2O_4$30% sample. The inset is the pore size distribution curve.

sorption branch of the N_2 isotherm as shown in the inset of Figure 9.

Figure 10 shows the magnetization measurement for the as-prepared $Bi_2O_2CO_3/CoFe_2O_4$ nanocomposites and pure $CoFe_2O_4$, using a vibrating sample magnetometer (VSM) at room temperature. The magnetization curves of the nanocomposites undoubtedly indicate ferromagnetism orders due to the presence of ferromagnetic $CoFe_2O_4$ nanoparticles. The saturation magnetization values of $Bi_2O_2CO_3/CoFe_2O_4$30%, $Bi_2O_2CO_3/CoFe_2O_4$45% and pure $CoFe_2O_4$ were found to be 17.15, 28.68 and 63.36 emu/g, respectively. The saturation magnetizations of the magnetic nanocomposites decrease compared with that of pure $CoFe_2O_4$, which can be attributed to the nano-magnetic $Bi_2O_2CO_3$ component. As demonstrated in the inset

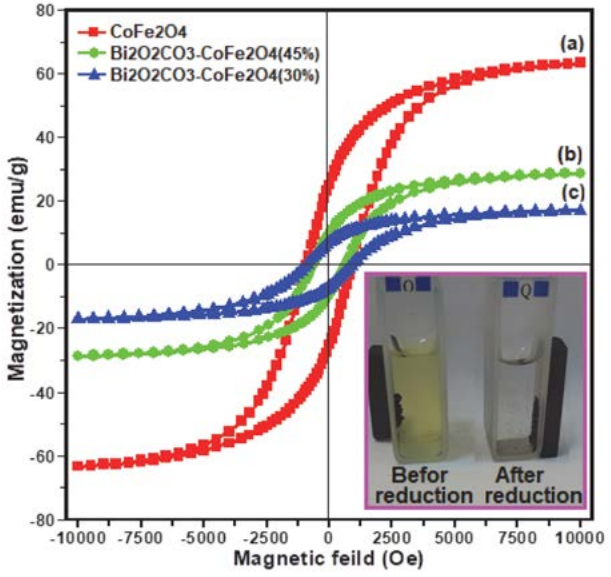

Figure 10. Magnetization curves of (a) pure $CoFe_2O_4$, (b) $Bi_2O_2CO_3/CoFe_2O_4$45% and (c) $Bi_2O_2CO_3/CoFe_2O_4$30%, The photo inset shows magnetic separation of the nanocomposite catalyst before and after the reduction of 4-NP by $NaBH_4$.

of Figure 10, complete separation of the catalyst colloids from the solution can be achieved under an external magnetic field. The rapid and easy magnetically separation of hybrid from water will assure the effective collection of the used catalysts and avoid the loss of nanoparticles for environmental risks.

3. 2. Catalytic Reduction of 4-Nitrophenol

To investigate the catalytic activity of $Bi_2O_2CO_3/CoFe_2O_4$ nanostructures with different contents of $CoFe_2O_4$, the reduction of 4-nitrophenol (4-NP) to 4-amiophenol (4-AP) by excess $NaBH_4$ in aqueous solution was used as the model reaction (Figure. 11). Usually, 4-NP solution exhibits a strong absorption peak at 317 nm and a weak shoulder peak at 400 nm in the region of 250–550 nm.[64] After alkali $NaBH_4$ is added into 4-NP solution, the absorption peak at 317 nm disappears; only the one at 400 nm exists and markedly increases, which should be attributed to the production of the intermediate state, 4-nitrophenolate ion.[65] The intermediate can stably exist for a couple of day still a catalyst is introduced into the above system. Here, the peak at 400 nm gradually decreases, and concomitantly, a new peak at 305 nm appears due to the production of 4-AP.[66,67] Figure 11(a) exhibits the UV–vis absorption spectra of the 4-NP-$NaBH_4$-H_2O system after reacting for various durations in the presence of 5 mg pure $Bi_2O_2CO_3$ nanostructures. One can easily find that the peak intensity at 400 nm markedly decreases with the prolonging of the reaction time and disappeared after 32 min. However, $Bi_2O_2CO_3$ nanostructures with different contents of $CoFe_2O_4$ exhibit different catalytic activities for the reduction of 4-NP. As shown in Figure 11(b), it merely took 20 min to completely convert 4-NP to 4-AP in the presence of $Bi_2O_2CO_3/CoFe_2O_4$30% nanocomposite. After the same amount of $Bi_2O_2CO_3/CoFe_2O_4$45% was used as the catalyst, it took 60 min to complete the reaction (Figure 11(c)). Namely, among various samples, $Bi_2O_2CO_3/CoFe_2O_4$30% bears the strongest catalytic activity. Introduction of $CoFe_2O_4$ in the composite significantly improves the catalytic activities of $Bi_2O_2CO_3$. However, an excess addition of $CoFe_2O_4$ showed decrease in catalytic efficiencies. In the present work, the reduction reaction of 4-NP to 4-AP could be reasonably assumed as a pseudo-first-order kinetics with regard to 4-NP owing to the presence of excess $NaBH_4$. This pseudo-first-order kinetics equation can be described as $\ln C_0/C_t = kt$. Here, C_0 and C_t represent the initial and instantaneous concentrations of 4-NP, respectively; and k and t stand for the apparent rate constant and the reaction time in turn. The apparent rate constant values were calculated from the slope of plot of ln (C_0/C_t) versus reaction time (Figure 11(d)). The apparent rate constant (k) value for the $Bi_2O_2CO_3/CoFe_2O_4$30% sample (0.20 min^{-1}) was estimated which is higher than $Bi_2O_2CO_3/CoFe_2O_4$45% (0.04 min^{-1}) and pure $Bi_2O_2CO_3$ (0.13 min^{-1}) samples. From the observed results, it was ev-

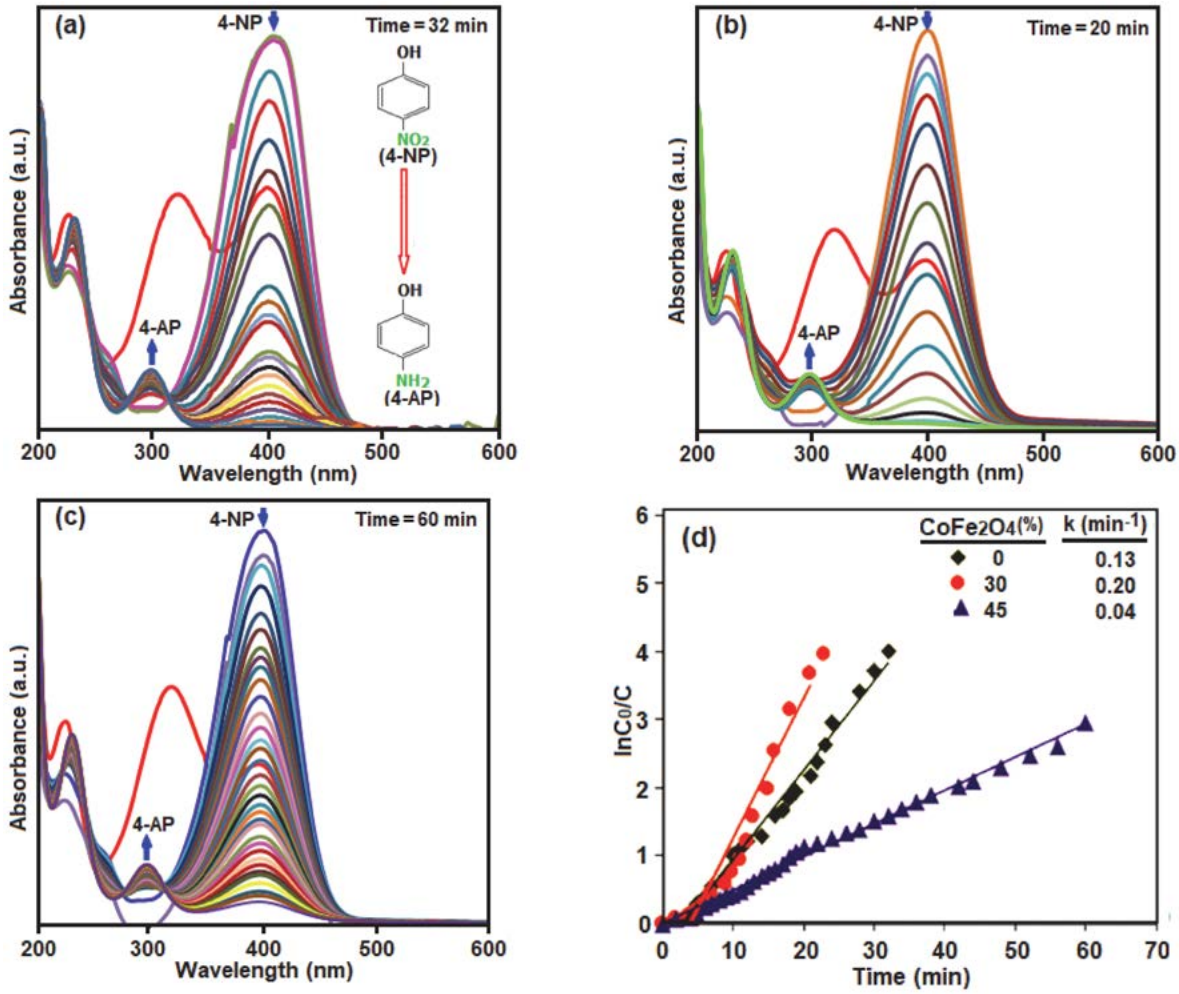

Figure 11. UV-vis spectral changes during the reduction of 4-NP with $NaBH_4$ over different catalysts: (a) pure $Bi_2O_2CO_3$, (b) $Bi_2O_2CO_3/CoFe_2O_4$30%, (c) $Bi_2O_2CO_3/CoFe_2O_4$45% and (d) Plot of $\ln(C_0/C_t)$ against the reaction time (the inset is the apparent rate constant values). Conditions: 4-NP (2 mL, 0.2 mM), catalyst (5.0 mg), $NaBH_4$ (0.5 mL, 20 mM), at 25 °C.

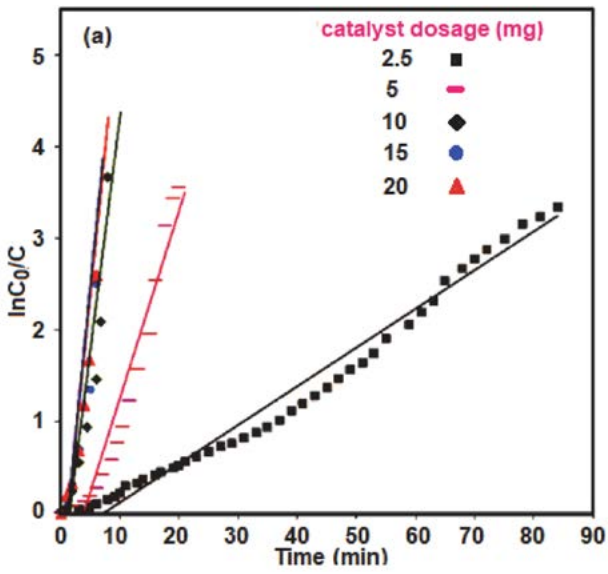

ident that the catalytic activity deteriorates with increasing $CoFe_2O_4$ content, showing that the loading percentage and intimate contact between two materials play an important role in determining catalytic efficiency. This means that with higher content of $CoFe_2O_4$ the number of the active catalytic reaction sites decreases and cause a negative influence on the catalytic processes. Excessive amount of

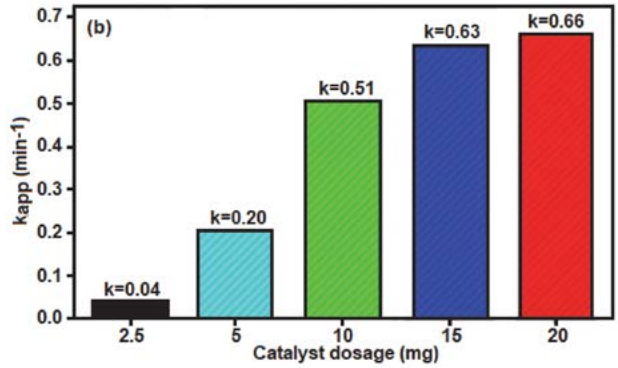

Figure 12 (a) Plot of ln (C_0/C) against the reaction time in the presence of different amounts of $Bi_2O_2CO_3/CoFe_2O_4$30% catalyst, and (b) the apparent rate constant values). Conditions: nitro compounds (2 mL, 0.2 mM) and $NaBH_4$ (0.5 mL, 20 mM), at 25 °C were used in all reactions.

$CoFe_2O_4$ may cover the active sites at the surface of $Bi_2O_2CO_3$ and also could hinder the contact with 4-NP. The highest catalytic performance of $Bi_2O_2CO_3/CoFe_2O_4$30% composite can be attributed to intimate contact between $Bi_2O_2CO_3$ and $CoFe_2O_4$ which facilitates the electron transfer. Moreover, the existence of $CoFe_2O_4$ in composites makes them magnetically separable during catalytic reactions.

The effect of the catalyst amount on the catalytic efficiency was investigated as well. Figure 12(a) shows linear relationships between $\ln(C_0/C_t)$ and the reaction time in the presence of different amounts of $Bi_2O_2CO_3/CoFe_2O_4$30% nanostructure. As shown in Figure 12(b), the rate constants (k_{app}) of 4-NP reduction reaction were calculated to be 0.04, 0.20, 0.51, 0.63 and 0.66 min^{-1} from the slope of the straight with various amount of $Bi_2O_2CO_3/CoFe_2O_4$30% catalyst. The k_{app} increased as the amount of $Bi_2O_2CO_3/CoFe_2O_4$30% catalyst increasing from 2.5 to 20 mg. A higher dosage of $Bi_2O_2CO_3/CoFe_2O_4$30% nanocomposite in the solution provides more active sites for the generation of H_2 and e^- (from $NaBH_4$), led to an increased reaction rate.

Furthermore, it was found that the present catalyst could also catalyze the reduction of other aromatic nitrocompounds including 4-nitroaniline (4-NA), 2-nitroaniline (2-NA) and 2-nitrophenol (2-NP), to corresponding amines. Figure 13(a)-(c) shows the reduction of three nitroarene by $NaBH_4$ in the presence of $Bi_2O_2CO_3/CoFe_2O_4$30% nanocomposite. The reductive reactions were completed within 15 min (for 4-NA), 29 min (for 2-NA) and 16 min (for 2-NP), respectively. The calculated reaction rate constants (k_{app}) for these substrates are displayed in Fig. 13(d). The k_{app} values of these substrates are as the following order: 4-NA (0.24 min^{-1}) > 2-NP (0.23 min^{-1}) >2-NA (0.1 min^{-1}). Since the reactions were carried out under the same experimental conditions, the different rates can be related to the structures of nitrocompounds.

In addition to catalytic activity, the stability and reusability of catalysts are important issues for their practical applications. The stability of as synthesized $Bi_2O_2CO_3/$

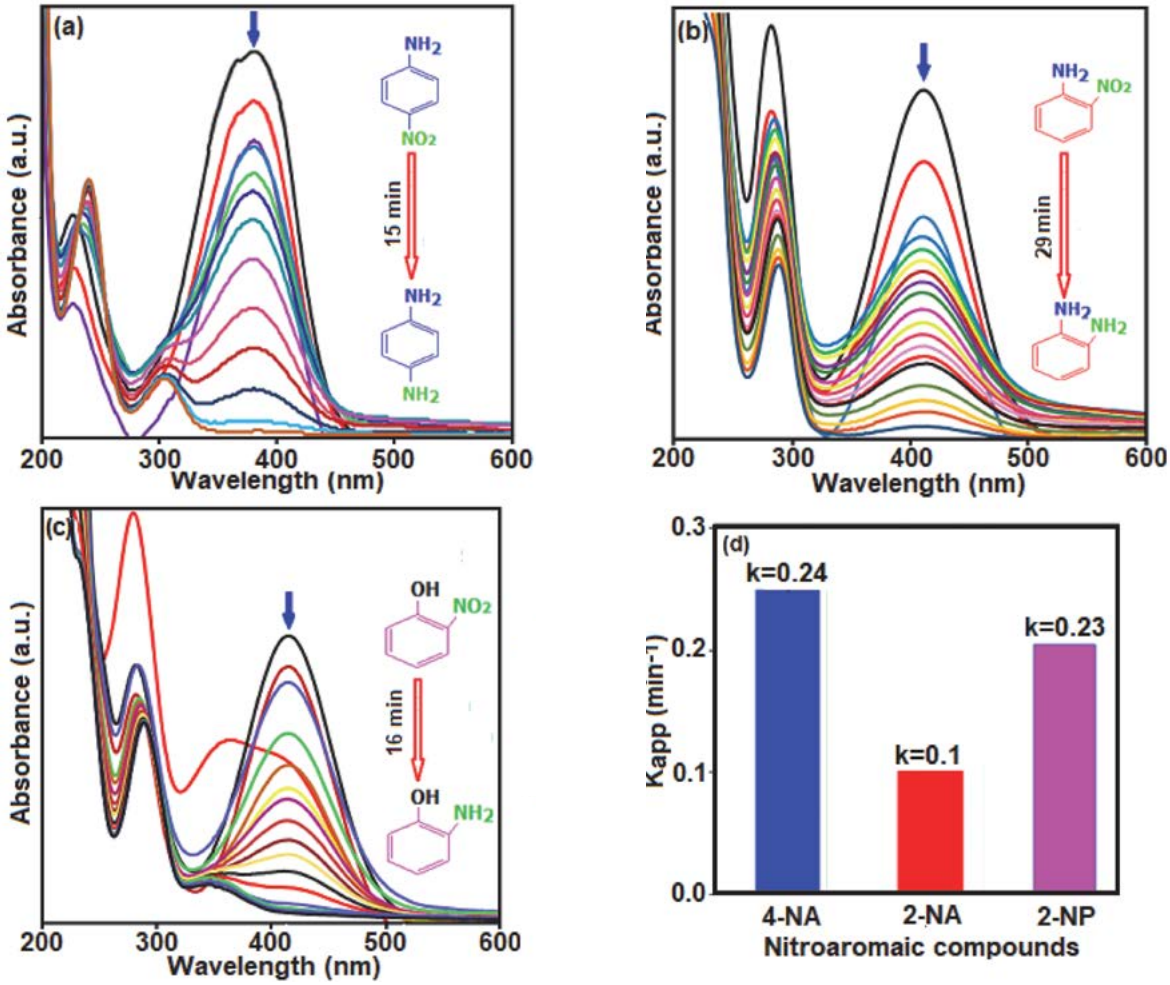

Figure 13. The UV–vis absorption spectra change for the reduction process of (a) 4-nitroaniline (4-NA), (b) 2-nitroaniline (2-NA), and (c) 2-nitrophenol (2-NP) with $NaBH_4$ in the presence of $Bi_2O_2CO_3/CoFe_2O_4$30% catalyst. (d) the calculated apparent rate constant values. Conditions: catalyst (5.0 mg), $NaBH_4$ (0.5 mL, 20 mM), and nitro compound (2 mL, 0.2 mM) at 25 °C.

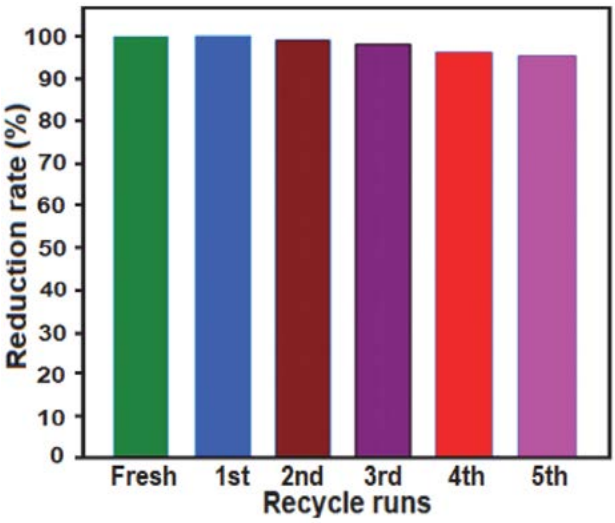

Figure 14. Recyclability of the of $Bi_2O_2CO_3/CoFe_2O_4$30% nanocomposite in the reduction of 4-NP. Conditions: catalyst (5.0 mg), [4-NP] = 0.2 mM and [$NaBH_4$] = 20 mM, at 25 °C.

$CoFe_2O_4$ 30% catalyst was checked by performing four consecutive cycles. The catalyst used in any experiment was collected by external magnetic field, washed with distilled water, dried at 60 °C and then employed for a new run without any observable weight loss. As shown in Figure 14, no significant loss of the catalytic activity can be observed after five successive runs of 4-NP reduction, indicating that the present composite catalysts are stable enough during the repeated experiments.

The nature of the recovered catalyst was also tested. As shown in Figure 15 (a) and (b), XRD pattern and FT-IR spectrum of the recycled $Bi_2O_2CO_3/CoFe_2O_4$30% nanocomposite catalyst did not show significant changes after the fourth run in comparison with the fresh catalyst (see Figures 1(c) and 2(c)). Figures 15(c) and (d) show the SEM and TEM images of the catalyst after five cycles, respectively. It could be observed that the recovered catalyst kept its initial size and morphology (see Figures 3(e)-(f) and 4) and the surface of $Bi_2O_2CO_3$ nanoplates was still decorated with $CoFe_2O_4$ nanoparticles, revealing the strong binding

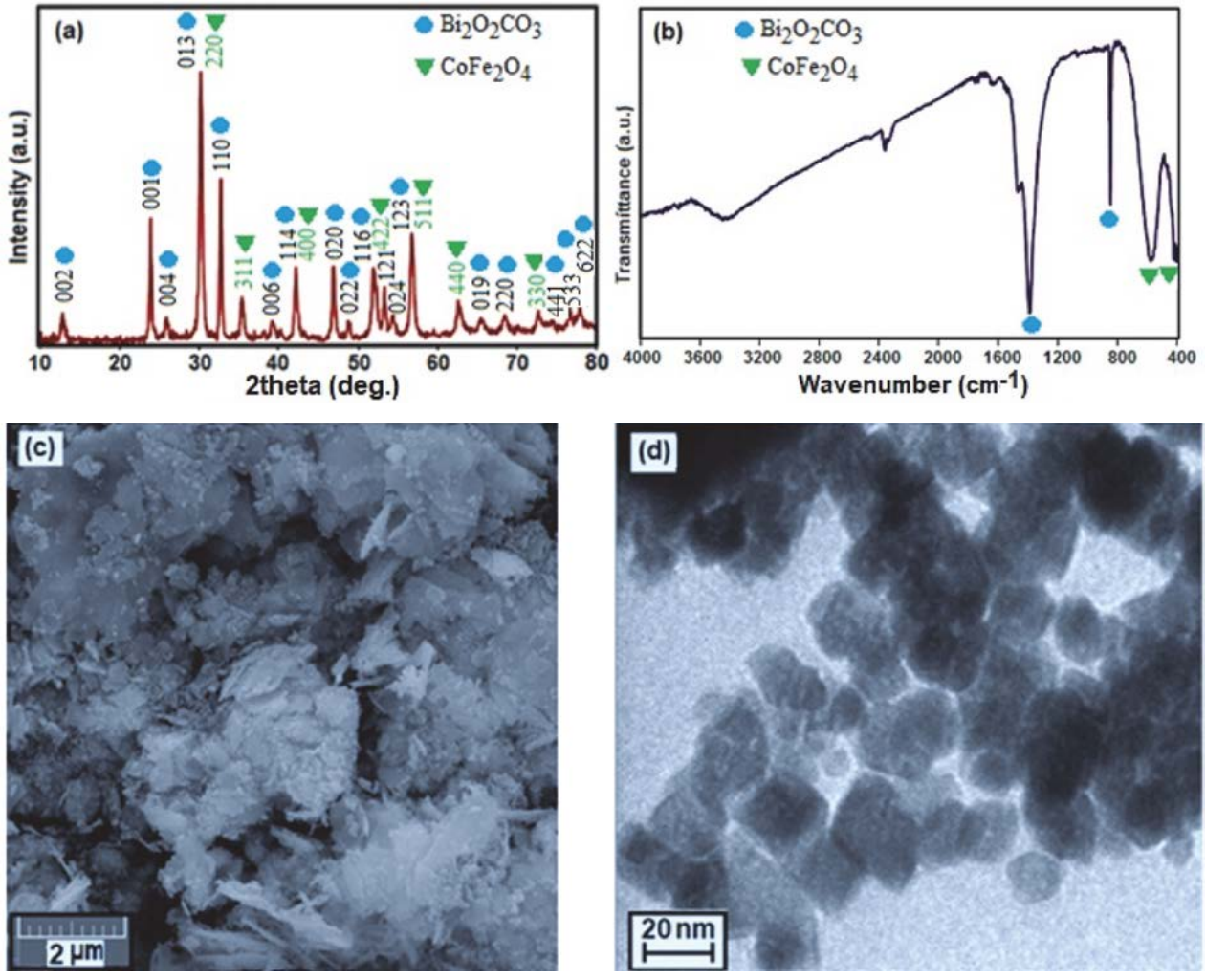

Figure 15. (a) XRD pattern, (b) FT-IR spectrum, (c) SEM image, and (d) TEM image of the recovered $Bi_2O_2CO_3/CoFe_2O_4$30% nanocomposite after the 5th run.

between the $CoFe_2O_4$ nanoparticles and $Bi_2O_2CO_3$ nanoplates. Therefore, the as-prepared $Bi_2O_2CO_3/CoFe_2O_4$ composites can work as an effective catalyst for the of reduction nitroaromatic compounds with good stability and recyclability.

In order to show the advantage of the present method, we have compared the obtained results in the reduction of 4-NP with $NaBH_4$ catalyzed by $Bi_2O_2CO_3/CoFe_2O_4$30% with some reported catalysts in the literature.[68–80] From Table 1, it is clear that with respect to the reaction conditions and/or reaction times, the present method is more suitable and/or superior. It is clear that reaction in the presence of most reported catalysts required longer reaction times (Table 1, entries 1–10). However, the present catalyst showed close or lower catalytic activity compared with some of the catalysts (Table 1, entries 11 and 12). Also, the results confirms that this magnetic catalyst has higher catalytic activity than that of the previously reported$Bi_2O_2CO_3/NiFe_2O_4$30% catalyst in the reduction of 4-nitrophenol to 4-aminophenol under same conditions (Table 1, entries 13 and 14). Furthermore, the present nanocomposite can be easily prepared in one-step without the use of harsh, toxic and expensive chemicals which is very important in practical applications.

4. Conclusions

To conclude, a series of novel plate–like $Bi_2O_2CO_3/CoFe_2O_4$ magnetic nanocomposites were successfully synthesized via a simple hydrothermal method for the first time and applied to catalyze the reduction of nitroarenes. Compared with the individual $Bi_2O_2CO_3$ and $CoFe_2O_4$, the composite catalysts exhibit higher catalytic performance and stability for 4-nitrophenol reduction under ambient conditions. Compared with those noble metals such as Au, Ag, Pt and Pd, $Bi_2O_2CO_3/CoFe_2O_4$ composites were easy to available and inexpensive. The preparation procedure of $Bi_2O_2CO_3/CoFe_2O_4$ magnetic nanocomposites via hydrothermal method was simple. And the as-prepared $Bi_2O_2CO_3/CoFe_2O_4$ magnetic nanocomposites were stable and well-dispersed. Moreover, the prepared $Bi_2O_2CO_3/CoFe_2O_4$ nanocomposites were magnetically separable from water with higher long-time use stability. This study provides a new approach for reducing and removing nitroarenes pollutants (e.g. 4-NP) in wastewater without introducing secondary pollutant into the system. Studies on the synthesis of nanocomposites of $Bi_2O_2CO_3$ with other ferrites (MFe_2O_4; M = Ni, Zn, Cu, Mn, …) and their thermal catalytic and photocatalytic applications are currently in progress and underway in our laboratory.

5. Acknowledgements

This work was supported by the Lorestan University Research Council and Iran Nanotechnology Initiative Council (INIC).

Table 1. Comparison of the result obtained for the complete reduction of 4-NP in the present work with those obtained by some reported catalysts.

Entry	Catalyst	Reaction conditions	Reaction time (min)	Ref.
1	Ni-PVA/SBA-15	H_2O, $NaBH_4$, r.t.	85	68
2	Hierarchical Au/CuO NPs	H_2O, $NaBH_4$, r.t	80	69
3	Cu NPs	THF/H_2O, $NaBH_4$, 50 °C	120	70
4	PdCu/graphene	EtOH/H_2O, $NaBH_4$, 50 °C	90	71
5	Au-GO	H_2O, $NaBH_4$, r.t.	30	72
6	$CoFe_2O_4$ NPs	H_2O, $NaBH_4$, r.t.	50	73
7	$FeNi_2$ nano-alloy	H_2O, $NaBH_4$, r.t	60	74
8	$NiCo_2$ nano-alloy	H_2O, $NaBH_4$, r.t.	30	75
9	CdS/GO	H_2O, $NaBH_4$, r.t.	30	76
10	dumbbell-like CuO NPs	H_2O, $NaBH_4$, r.t.	32	77
11	Ni NPs	H_2O, $NaBH_4$, r.t.	16	78
12	$CuFe_2O_4$ NPs	H_2O, $NaBH_4$, r.t.	14	79
13	$Bi_2O_2CO_3/NiFe_2O_4$30%	H_2O, $NaBH_4$, r.t.	42	80
14	$Bi_2O_2CO_3/CoFe_2O_4$30%	H_2O, $NaBH_4$, r.t.	20	This work

6. References

1. J. R. Chiou, B. H. Lai, K. C. Hsu and D. H. Chen, *J. Hazard. Mater*. **2013**, *248*, 394–400. **DOI:**10.1016/j.jhazmat.2013.01.030
2. Y. Shaoqing, H. Jun and W. Jianlong, *Radiat. Phys. Chem.* **2010**, *79*, 1039–1046. **DOI:**10.1016/j.radphyschem.2010.05.008
3. A. C. Apolinario, A. M. Silva, B. F. Machado, H. T. Gomes, P. P. Araujo, and J. L. Figueredo, *Appl. Catal. B: Environ*. **2008**, *84*, 75–86. **DOI:**10.1016/j.apcatb.2007.12.018
4. V. Maurino, C. Minero, E. Pelizzetti, P. Piccinini, N. Serpone

and H. Hidaka, *J. Photochem. Photobiol. A: Chem*. **1997**, *109*, 171–176. **DOI:**10.1016/S1010-6030(97)00124-X
5. P. Xiong, Y. Fu, L. Wang and X. Wang, *J. Chem. Eng*. **2012**, *195*, 149–157. **DOI:**10.1016/j.cej.2012.05.007
6. F. R. Zaggout and N. A. Ghalwa. *J. Environ. Manag.* **2008**, *86*, 291–296. **DOI:**10.1016/j.jenvman.2006.12.033
7. X. Zhu and J. Ni, *Electrochim. Acta*, **2011**, *56*, 10371–10377. **DOI:**10.1016/j.electacta.2011.05.062
8. Y. Y. Chu, Y. Qian, W. J. Wang and X. Deng, *J. Hazard. Mater.* **2012**, *199*, 179–185. **DOI:**10.1016/j.jhazmat.2011.10.079
9. C. Rizhi, D. Yan, X. Weihong and X. Nanping, *Chin. J. Chem. Eng.* **2007**, *15*, 884–888. **DOI:**10.1016/S1004-9541(08)60019-1
10. Z. Wu, J. Chen, Q. Di and M. Zhang, *Catal. Commun.* **2012**, *18*, 55–59. **DOI:**10.1016/j.catcom.2011.11.015
11. Y. Du, H. Chen, R. Chen and N. Xu, *Appl. Catal. A: Gen.* **2004**, *277*, 259–264. **DOI:**10.1016/j.apcata.2004.09.018
12. K. I. Min, J. S. Choi, Y. M. Chung, W. S. Ahn, R. Ryoo and P. K. Lim, *Appl. Catal. A: Gen.* **2008**, *337*, 97–104. **DOI:**10.1016/j.apcata.2007.12.004
13. T. Aditya, A. Pal and T. Pal, *Chem. Commun.* **2015**, *51*, 9410–9431 and reference cited therein.
14. T. R. Mandlimath and B. Gopal, *J. Mol. Catal A: Chem.* **2011**, *350*, 9–15. **DOI:**10.1016/j.molcata.2011.08.009
15. Y. C. Chang and D. H. Chen, *J. Hazard. Mater.* **2009**, *165*, 664–669. **DOI:**10.1016/j.jhazmat.2008.10.034
16. Y. Deng, Y. Cai, Z. Sun, J. Liu, C. Liu, J. Wei, W. Li, C. Liu, Y. Wang and D. Y. Zhao, *J. Am. Chem. Soc.* **2010**, *132*, 8466–8473. **DOI:**10.1021/ja1025744
17. S. Harish, J. Mathiyarasu, K. Phani and V. Yegnaraman, *Catal. Lett.* **2009**, *128*, 197–202. **DOI:**10.1007/s10562-008-9732-x
18. J. Huang, S. Vongehr, S. Tang, H. Lu, J. Shen and X. Meng, *Langmuir*, **2009**, *25*, 11890–11896. **DOI:**10.1021/la9015383
19. H. Koga and T. Kitaoka, *J. Chem. Eng.* **2011**, *168*, 420–425. **DOI:**10.1016/j.cej.2010.08.073
20. P. Liu and M. Zhao, *Appl. Surf. Sci.* **2009**, *255*, 3989–3993. **DOI:**10.1016/j.apsusc.2008.10.094
21. J. Wang, X. B. Zhang, Z. L. Wang, L. M. Wang, W. Xing and X. Liu, *Nanoscale*, **2012**, *4*, 1549–1552. **DOI:**10.1039/c2nr11912a
22. Y. Zhu, J. Shen, K. F. Zhou, C. Chen, X. Yang and C. Li, *J. Phys. Chem. C*, **2010**, *115*, 1614–1619. **DOI:**10.1021/jp109276q
23. F. H. Lin and R. A. Doong, *J. Phys. Chem. C*, **2011**, *115*, 6591–6598. **DOI:**10.1021/jp110956k
24. K. Jiang, H. X. Zhang, Y. Y. Yang, R. Mothes, H. Lang and W. B. Cai, *Chem. Commun.* **2011**, *47*, 11924–11926. **DOI:**10.1039/c1cc14675k
25. H. He and C. Gao, *J. Nanomater.* **2011**, *2011*, 1–10.
26. X. Du, J. He, J. Zhu, L. Sun and S. An, *Appl. Surf. Sci.* **2012**, *258*, 2717–2723. **DOI:**10.1016/j.apsusc.2011.10.122
27. D. Y. Li, Y. G. Zhang, Y. L. Zhang, X. F. Zhou and S. J. Guo, *J. Hazard. Mater.* **2013**, *258–259*, 42–49. **DOI:**10.1016/j.jhazmat.2013.02.058
28. R. G. Li, F. X. Zhang, D. G. Wang, J. X. Yang, M. R. Li, J. Zhu, X. Zhou, H. X. Han and C. Li, *Nat. Commun.* **2013**, *4*, 1432. **DOI:**10.1038/ncomms2401
29. S. M. Sun, W. Z. Wang and L. Zhang, *J. Phys. Chem. C*, **2013**,*117*, 9113–9120. **DOI:**10.1021/jp4004592
30. G. H. Tian, Y. J. Chen, W. Zhou, K. Pan, Y. Z. Dong, C. G. Tian and H. G. Fu, *J. Mater. Chem.* **2011**, *21*, 887–892. **DOI:**10.1039/C0JM03040F
31. X. Zhao, J. H. Qu, H. J. Liu and C. Hu, *Environ. Sci. Technol.* **2007**, *41*, 6802–6807. **DOI:**10.1021/es070598b
32. J. Jiang, K. Zhao, X. Y. Xiao and L. Z. Zhang, *J. Am. Chem. Soc.* **2012**, *134*, 4473–4476. **DOI:**10.1021/ja210484t
33. Y. N. Wang, K. J. Deng and L. Z. Zhang, *J. Phys. Chem. C*, **2011**, *115*, 14300–14308. **DOI:**10.1021/jp2042069
34. L. Ye, J. Liu, C. Gong, L. Tian, T. Peng and L. Zan, *ACS Catal.* **2012**, *2*, 1677–1683. **DOI:**10.1021/cs300213m
35. Z. Ni, Y. Sun, Y. Zhang and F. Dong, *Appl. Surf. Sci.* **2016**, *365*, 314–335. **DOI:**10.1016/j.apsusc.2015.12.231
36. R. Hu, X. Xiao, S. Tu, X. Zuo and J. Nan, *Appl. Catal. B: Environ.* **2015**, *163*, 510–519. **DOI:**10.1016/j.apcatb.2014.08.025
37. Q. Wang, G. Yun, Y. Bai, N. An, J. Lian, H. Huang and B. Su, *Appl. Surf. Sci.* **2014**, *313*, 537–544. **DOI:**10.1016/j.apsusc.2014.06.018
38. H. Lu, L. Xu, B. Wei, M. Zhang, H. Gao and W. Sun, *Appl. Surf. Sci.* **2014**, *303*, 360–366. **DOI:**10.1016/j.apsusc.2014.03.006
39. N. Guo, Y. Cao, Y. Rong and D. Jia, *RSC Adv.* **2016**, *6*, 106046–106053
40. J. Cao, X. Li, H. Lin, S. Chen and X. Fu, *J. Hazard. Mater.* **2012**, *239*, 316–324. **DOI:**10.1016/j.jhazmat.2012.08.078
41. X. Huang and H. Chen, *Appl. Surf. Sci.* **2013**, *284*, 843–848. **DOI:**10.1016/j.apsusc.2013.08.019
42. N. Liang, J. Zai, M. Xu, Q. Zhu, X. Wei and X. Qian, *J. Mater. Chem. A*, **2014**, *2*, 4208–4216. **DOI:**10.1039/c3ta13931j
43. Y. Ao, L. Xu, P. Wang, C. Wang, J. Hou and J. Qian, *Dalton Trans.*, **2015**, *44*, 11321–11330. **DOI:**10.1039/C5DT01168J
44. Y. Liu, P. Zhang, H. Lv, J. Guang, S. Li and J. Jiang, *RSC Adv.* **2015**, *5*, 83764–83772.
45. Q. Zhang, H. Y. Wang, S. Z. Hu, G. Lu, J. Bai, X. X. Kang, D. Liu and J. Z. Gui, *RSC Adv.* **2015**, *5*, 42736–42743.
46. N. Liang, M. Wang, L. Jin, S. S. Huang, W. L. Chen, M. Xu, Q. Q. He, J. T. Zai, N. H. Fang and X. F. Qian, *ACS Appl. Mater. Interfaces*, **2014**, *6*, 11698–11705. **DOI:**10.1021/am502481z
47. L. Jin, G. Q. Zhu, M. Hojamberdiev, X. C. Luo, C. W. Tan, J. H. Peng, X. M. Wei, J. P. Li and P. Liu, *Ind. Eng. Chem. Res.* **2014**, *53*, 13718–13727. **DOI:**10.1021/ie502133x
48. Y. Hu, C. Dong, K. L. Wu, S. H. Xia, X. Li and X. W. Wei, *Mater. Lett.* **2015**, *147*, 69–71. **DOI:**10.1016/j.matlet.2014.12.097
49. T. Li, X. Hu, C. Liu, C. Tang, X. Wang and S. Luo, *J. Mol. Catal. A: Chem.* **2016**, *425*, 124–135. **DOI:**10.1016/j.molcata.2016.10.001
50. X. Zhang, S. Li, S. Hua, J. Chen, W. Jiang, J. Zhang, L. Ji, L. Cai, Y. Wang, W. Song and J. Liu, *Mater. Lett.* **2016**, *185*, 50–53. **DOI:**10.1016/j.matlet.2016.08.086
51. S. Shylesh, V. Schunemann, and W. R. Thiel, *Angew. Chem., Int. Ed.* **2010**, *49*, 3428–3459. **DOI:**10.1002/anie.200905684
52. X. F. Shang, W. C. Lu, B. H. Yue, L. M. Zhang, J. P. Ni, Y. Lv and Y. L. Feng, *Cryst. Growth Des.* **2009**, *9*, 1415 –1420. **DOI:**10.1021/cg800730s

53. G. E. Tobon-Zapata, S. B. Etcheverry and E. J. Baran, *J. Mater. Sci. Lett.* **1997**, *16*, 656–657. **DOI:**10.1023/A:1018527602604
54. Y. S. Fu and X. Wang, *Ind. Eng. Chem. Res.* **2011**, *50*, *7210*–7218. **DOI:**10.1021/ie200162a
55. G. D. Hong, Y. Yamada, T. Nagatomi, Y. Takai and S. Fukuzumi, *J. Am. Chem. Soc*. **2012**, *134*, 19572–19575. **DOI:**10.1021/ja309771h
56. K. Modi, S. Shah, N. Pujara, T. Pathak, N. Vasoya and I. Jhala, *J. Mol. Struct.*, **2013**, *1049*, 250–262. **DOI:**10.1016/j.molstruc.2013.06.051
57. J. Gunjakar, A. More, K. Gurav and C. Lokhande, *Appl. Surf. Sci.*, **2008**, *254*, 5844–5848 **DOI:**10.1016/j.apsusc.2008.03.065
58. Y. C. Huang, W. J. Fan, B. Long, H. B. Li, F. Y. Zhao, Z. L. Liu, Y. X. Tong and H. B. Ji, *Appl. Catal. B: Environ.* **2015**, *185*, 68–76. **DOI:**10.1016/j.apcatb.2015.11.043
59. D. D. Hu, K.Y. Zhang, Q. Yang, M. J. Wang, Y. Xi and C. G. Hu, *Appl. Surf. Sci.*, **2014**, *316*, 93–101. **DOI:**10.1016/j.apsusc.2014.07.185
60. H. J. Lu, L. L. Xu, B. Wei, M. Y. Zhang, H. Gao and W. J. Sun, *Appl. Surf. Sci.* **2014**, *303*, 360–366. **DOI:**10.1016/j.apsusc.2014.03.006
61. S. Singh and N. Khare, *RSC Adv.* **2015**, 5, 96562–96572.
62. P. Madhusudan, J. Yu, W. Wang, B. Cheng and G. Liu, *Dalton Trans.* **2012**, *41*, 14345–14353. **DOI:**10.1039/c2dt31528a
63. L. Xu, X. Yang, Z. Zhai and W. Hou, *CrystEngCommun.* **2011**, *13*, 7267–7275. **DOI:**10.1039/c1ce05671a
64. Z. Jin, M. Xiao, Z. Bao, P. Wang and J. Wang, *Angew. Chem., Int. Ed.* **2012**, *51*, 6406–6410. **DOI:**10.1002/anie.201106948
65. A. K. Patra, A. Dutta and A. Bhaumik, *Catal. Commun.* **2010**, *11*, 651–655. **DOI:**10.1016/j.catcom.2010.01.015
66. H. Li, J. K. Jo, L. Zhang, C. S. Ha, H. Suh and I. Kim, *Adv. Funct. Mater*. **2010**, *20*, 3864–3873. **DOI:**10.1002/adfm.201001067
67. M. Nemanashi and R. Meijboom, *J. Colloid Interface Sci.*, **2013**, *389*, 260–267. **DOI:**10.1016/j.jcis.2012.09.012
68. R. J. Kalbasi, A. A. Nourbakhsh and F. Babaknezhad, *Catal. Commun.* **2011**, *12*, 955–960. **DOI:**10.1016/j.catcom.2011.02.019
69. S. Y. Gao, X. X. Jia, Z. D. Li and Y. L. Chen, *J. Nanopart. Res.* **2012**, *14*, 1–11.
70. Z. Duan, G. Ma and W. Zhang, *Bull. Korean Chem. Soc.* **2012**, *33*, 4003–4006. **DOI:**10.5012/bkcs.2012.33.12.4003
71. A. K. Shil, D. Sharma, N. R. Guha, and P. Das, *Tetrahedron Lett*. **2012**, *53*, 4858–4861. **DOI:**10.1016/j.tetlet.2012.06.132
72. Y. Choi, H. S. Bae, E. Seo, S. Jang, K. H. Park and B. S. Kim, *J. Mater. Chem.* **2011**, *21*, 15431–15436. **DOI:**10.1039/c1jm12477c
73. M. Nasrollahzadeh, M. Bagherzadeh and H. Karimi, *J. Colloid Interface Sci*. **2016,** *465*, 271–278. **DOI:**10.1016/j.jcis.2015.11.074
74. K. L. Wu, R. Yu and X. W. Wei, *Cryst. Eng. Commun*. **2012,** *14*, 7626–7632. **DOI:**10.1039/c2ce25457c
75. K. L. Wu, X. W. Wei, X. M. Zhou, D. H. Wu, X. W. Liu, Y. Ye and Q. Wang, *J. Phys. Chem. C*. **2011**, *115*, 16268–16274. **DOI:**10.1021/jp201660w
76. S. Liu, Z. Chen, N. Zhang, Z. R. Tang and Y. J. Xu, *J. Phys. Chem. C*. **2013**, *117*, 8251–8261. **DOI:**10.1021/jp400550t
77. W. Che, Y. Ni, Y. Zhang and Y. Ma, *J. Phys. Chem. Solid*. **2015**, *77*, 1–7. **DOI:**10.1016/j.jpcs.2014.09.006
78. D. Z. Jiang, J. Xie, D. Jiang, X. Wei and M. Chen, *Cryst. Eng. Comm.* **2013**, *15*, 560–569. **DOI:**10.1039/C2CE26398J
79. J. Feng, L. Su, Y. Ma, C. Ren, Q. Guo and X. Chen, *Chem. Eng. J.* **2013**, *221*,16–24. **DOI:**10.1016/j.cej.2013.02.009
80. P. Zarringhadam and S. Farhadi, *J. Alloys Compd.* **2017**, *729*, 1046–1057. **DOI:**10.1016/j.jallcom.2017.09.247

Povzetek

Nove magnetne nanodelce $Bi_2O_2CO_3/CoFe_2O_4$ smo pripravili s hidrotermalno sintezo. Infrardečo spektroskopijo (FT-IR), rentgensko difrakcijo (XRD), vrstično elektronsko mikroskopijo (SEM), energijsko disperzivno spektroskopijo rentgenskih žarkov (EDX), presevno elektronsko mikroskopijo (TEM), rentgensko fotoelektronsko spektroskopijo (XPS), UV-Vis difuzno refleksijsko spektroskopijo (DRS), magnetometer z vibrirajočim vzorcem (VSM) in adsorpcijsko desorpcijsko analizo N_2 smo uporabili za preučevanje strukture, morfologije, velikosti delcev, fazne sestave, optičnih in magnetnih lastnosti sintetiziranih nanokompozitov. Rezultati karakterizacije vzorcev so pokazali uspešno vezavo sferičnih nanodelcev $CoFe_2O_4$ in ploščam podobnih nanostruktur $Bi_2O_2CO_3$. Katalitično aktivnost magnetnih nanokampozitov $Bi_2O_2CO_3/CoFe_2O_4$ smo ocenili z redukcijo nekaterih aromatičnih nitro-spojin, kot so nitrofenoli in nitroanilini, z uporabo vodne raztopine natrijevega borhidrida ($NaBH_4$) pri sobni temperaturi. Nanokampozit $Bi_2O_2CO_3/CoFe_2O_4$ s 30 % $CoFe_2O_4$ je pokazal najboljše rezultate pri redukciji aromatskih nitro spojin s popolno pretvorbo v ustrezne amino spojine v 15–30 minutah s konstanto hitrostjo 0,10–0,24 min^{-1}. Poleg tega lahko magnetni nanokompozit $Bi_2O_2CO_3/CoFe_2O_4$ zlahka odstranimo iz reakcijskega sistema z uporabo zunanjega magneta.